H_∞-Based Double Grid Forming Controller of Multi-Modular Converters in a Hybrid AC/DC Grid

Baron-Prada Eder
Automatic Control Laboratory
ETH Zurich, AIT
Vienna, Austria
ebaron@ethz.ch

Anta Adolfo, Makoschitz Markus
Electric Energy Systems
AIT
Vienna, Austria
adolfo.anta, markus.makoschitz@ait.ac.at

Dörfler Florian
Automatic Control Laboratory
ETH Zurich
Zurich, Switzerland
dorfler@ethz.ch

2023 IEEE 24th Workshop on Control and Modeling for Power Electronics (COMPEL) | 979-8-3503-1618-6/23/$31.00 ©2023 IEEE | DOI: 10.1109/COMPEL52896.2023.10221196

***Abstract*—The power system is witnessing an increasing penetration of power converters due to the integration of renewables, HVDC, DC and AC microgrids, etc. In line with this increasing penetration, the system needs units with grid-forming capabilities on the AC and DC sides. We propose a dual grid forming controller for power converters, particularly for modular multilevel converters (MMC), that forms the voltage in the DC grid and voltage and frequency on the AC grid. Nowadays, the parameter tuning of MMC controllers heavily relies on manual effort and rich engineering experience, which usually leads to suboptimal power system operation. Instead, we propose an optimal H_∞ controller, which considers AC and DC grid dynamics. We impose grid-forming conditions, among other control objectives, by using weighting functions. Finally, using a simple AC/DC grid we demonstrate that the proposed double grid forming algorithm is suitable for hybrid grid applications.**

***Index Terms*—H-infinity control, power converters, Dual grid-forming control, Hybrid grids, Multi Modular Converter.**

I. Introduction

The integration of inverter interfaced generation and the retirement of traditional power plants pose significant challenges to power system operation, given that a stiff AC voltage and frequency is no longer an accurate assumption in today's power systems. In this regard, grid-forming controllers address some of these issues, given their ability to form a stable grid and provide fast reactions against perturbations in the power system [1]. Most works have focused on grid-forming conditions either for the AC or DC grid. Double grid forming control has been proposed only recently [2] with promising results to address issues concerning to stability and reliability of hybrid AC/DC grids. Generally, grid-forming control strategies use several common assumptions in power systems, such as decoupling frequency and voltage or linearization of power flows [3].

In light of such challenges in grid-forming control, this paper develops a novel control strategy that simultaneously forms the DC and AC sides using a H_∞ controller utilizing weighting functions. H_∞ control is a robust control methodology that aims to design controllers to achieve optimal performance and stability in the presence of uncertainties and disturbances [4]. We define the static and dynamic controller objectives and how aggressively the controller behaves to meet such objectives. Meanwhile, the H_∞ control reduces the control effort over the system by optimally coordinating multiple inputs and outputs. Furthermore, the H_∞ control design used in this paper is compatible with standard PI controllers used in current control loops.

In this work we focus on MMC topologies, that are increasingly used in high-voltage DC transmission systems due to their ability to provide superior power quality, reduced harmonic distortion, and improved fault tolerance. One of the key features that set MMCs apart from other converter topologies is their submodules' capacitances, which enable them to function as double grid-forming devices under power balance conditions or even with a power unbalance for a short time [4]. The active use of the MMC capacitances enables fast response during transient events, stabilizing voltage and frequency. They also facilitate active power exchange and flexibility in grid operations, adapting to varying load demands and renewable energy availability. This feature means that MMCs can regulate both the voltage and frequency of the AC grid, making them a versatile and powerful tool for power system control. In this way, MMCs have emerged as a promising solution for the integration of renewable energy sources and the development of more resilient and flexible power grids.

Summarizing, in this paper we are proposing a robust control technique for the development of a double grid forming controller for AC/DC grid. We are utilizing weighting functions to actively achieve multiple objectives within the controller, enhancing its overall performance. We show that our H_∞-optimal controller applied to MMCs has adequate performance against variable grid conditions on the AC and DC side.

II. Hybrid AC/DC Grid Modelling

We consider an AC/DC grid, as illustrated conceptually in Figure 1, where the H_∞ controller is designed to provide effective voltage (AC and DC) and frequency (AC) control. Our model consists of a hybrid AC and DC system interconnected through a converter, which is a basic building block in every voltage level.

This work has been funded by the InnoCyPes project, which has received funding from the European Union's Horizon 2020 research and innovation programme under the Marie Skłodowska-Curie grant agreement No 956433.

A. AC and DC grid

The AC grid is assumed to be connected to the inverter through an LCL filter. To accurately represent the AC grid, a center of inertia modeling (CoI) approach is employed [5]. The CoI model relies on a weighted average of the rotational energies of all generators in the system, leading to an aggregated swing equation. It serves as the rotation point for the entire system, influencing its response to frequency changes and overall stability [6].

The DC grid is modeled as in [7], and it is composed of a resistance, an inductance, a capacitance, and a DC source, as is shown in Figure 2. Moreover, the aforementioned DC grid is connected to a DC node, featuring a parallel combination of capacitance, susceptance, and a current source. This configuration models a controllable energy source, such as a Battery Energy Storage System (BESS) or a PV generator with a storage device. By incorporating this setup, the approach maintains its versatility and accommodates a wide range of scenarios.

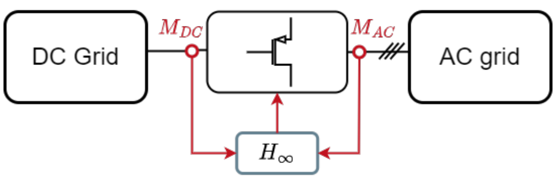

Fig. 1: Interconnection AC/DC system with a MMC in closed loop with a H_∞ controller.

B. Multi-Modular Converter (MMC) Modelling

For this work, we have selected a Multi Modular Converter (MMC) as the inverter, which consists of 6 arms, two for each phase. To simplify the analysis, we utilize a reduced model that assumes a balanced load condition, where the modulation signal of the AC phases is phase-shifted by 120º [2]. In line with the balanced grid, the arms of the same phase should store equal voltage and energy, controlled by the current control loops [2]. The internal dynamics of the MMC can be described by the following equations [8]:

$$L_{\text{eq}} I_3 \frac{\mathrm{d}}{\mathrm{d}t} i_s^{abc} = -R_{\text{eq}} I_3 i_s^{abc} + v_{\text{diff}}^{abc} - v_{\text{PCC}}^{abc} \tag{1}$$

$$C_{\text{eq}} I_3 \frac{\mathrm{d}}{\mathrm{d}t} u^{abc} = i_s^{abc} - i_{ac}^{abc} \tag{2}$$

$$2L_a I_3 \frac{\mathrm{d}}{\mathrm{d}t} i_{\text{sum}}^{abc} = -2R_a I_3 i_{\text{sum}}^{abc} + \mathbf{1}_3 v_{\text{dc}} - v_{\text{sum}}^{abc} \tag{3}$$

Here, $L_{eq} = L_s + L_a/2$ and $R_{eq} = R_s + R_a/2$, with $Z_{dc} = Z_{inv} = R_{eq} + jL_{eq}$. where R_a and L_a are the arm resistance and inductance, and R_s and L_s are the phase reactor resistance and inductance [2]. The currents i_s and i_{sum} are defined as $i_s = i_u - i_l$ and $i_{sum} = 1/2(i_u + i_l)$, where the sub-indices u and l refer to the upper and lower MMC arm, respectively. The voltages v_{diff} and v_{sum} are defined as $v_{diff} = 1/2(-v_u + v_l)$ and $v_{sum} = v_u + v_l$. By introducing an additional appropriate variable changes, the MMC can be modeled as a conventional converter. The macroscopic model, initially proposed in [9] for controller synthesis, represents the MMC as two controllable voltage sources in parallel with a capacitance that allows power provision based on the network condition, as shown in Figure 2.

To address grid forming dynamics and ensure fast and accurate voltage control, we assume the adequate response of internal arm and phase balancing controls and current controls [2]. As a result, we can simplify our model by neglecting the dynamics related to the current flowing in the arms described in (1) and (3). The macroscopic MMC model can then be written as:

$$C_{eq}\dot{v}_{dc} = i_{dc} - i_{ac} \tag{4}$$

$$\dot{W} = P_{dc} - P_{ac} = 3V_{dc}i_{dc} - \frac{3}{2}V_{ac}i_{ac}^{*} \tag{5}$$

Here, C_{eq} represents the equivalent capacitance and W is the energy stored in C_{eq}. In this simplified model, the MMC is considered lossless, and its dynamics are governed solely by the power input and output. Thus, the macroscopic MMC can be modeled as a DC-DC and AC-DC converter connected through a DC link with the equivalent capacitance, as illustrated in Figure 2.

Finally, the duty cycle of the equivalent DC-DC converter (α_{DC}) must be within the limits of the duty cycle of the equivalent DC-AC converter (α_{AC}), satisfying the following boundary conditions [9]:

$$2|\alpha_{AC}| < \alpha_{DC} < 2(1 - |\alpha_{AC}|)$$
$$0 < \alpha_{AC} < \frac{\alpha_{DC}}{2}$$

By making these compromises in our model, we have arrived at a reduced model that allows us to implement a grid forming source for both grids.

III. H_∞ Control Design

This section presents how to design a controller based on H_∞ methods considering grid forming objectives in both grids. First, an introduction on grid forming objectives and H_∞ control is given, and afterwards we describe how to enforce such objectives by the use of weighting functions.

A. Definitions and Preliminaries

1) H_∞ norm: The H_∞ norm, denoted as $|G(j\omega)|_\infty = \max_{\omega\in\mathbb{R}} \overline{\sigma}(G(j\omega))$, with $\overline{\sigma}$ denoting the maximum singular value, is a mathematical measure used in control theory to quantify the performance of a system in the frequency domain. It characterizes the worst-case gain from an input signal to an output signal over all frequencies. In $\mathcal{H}_\infty$ control, the goal is to design controllers that minimize the H_∞ norm of the transfer function between the exogenous disturbance signals and the controlled output signals, while satisfying certain performance and stability criteria. The H_∞ norm can be computed using optimization techniques such as linear matrix inequalities (LMIs) and is commonly used in robust control design to ensure robust stability and performance in the presence of uncertainties and disturbances.

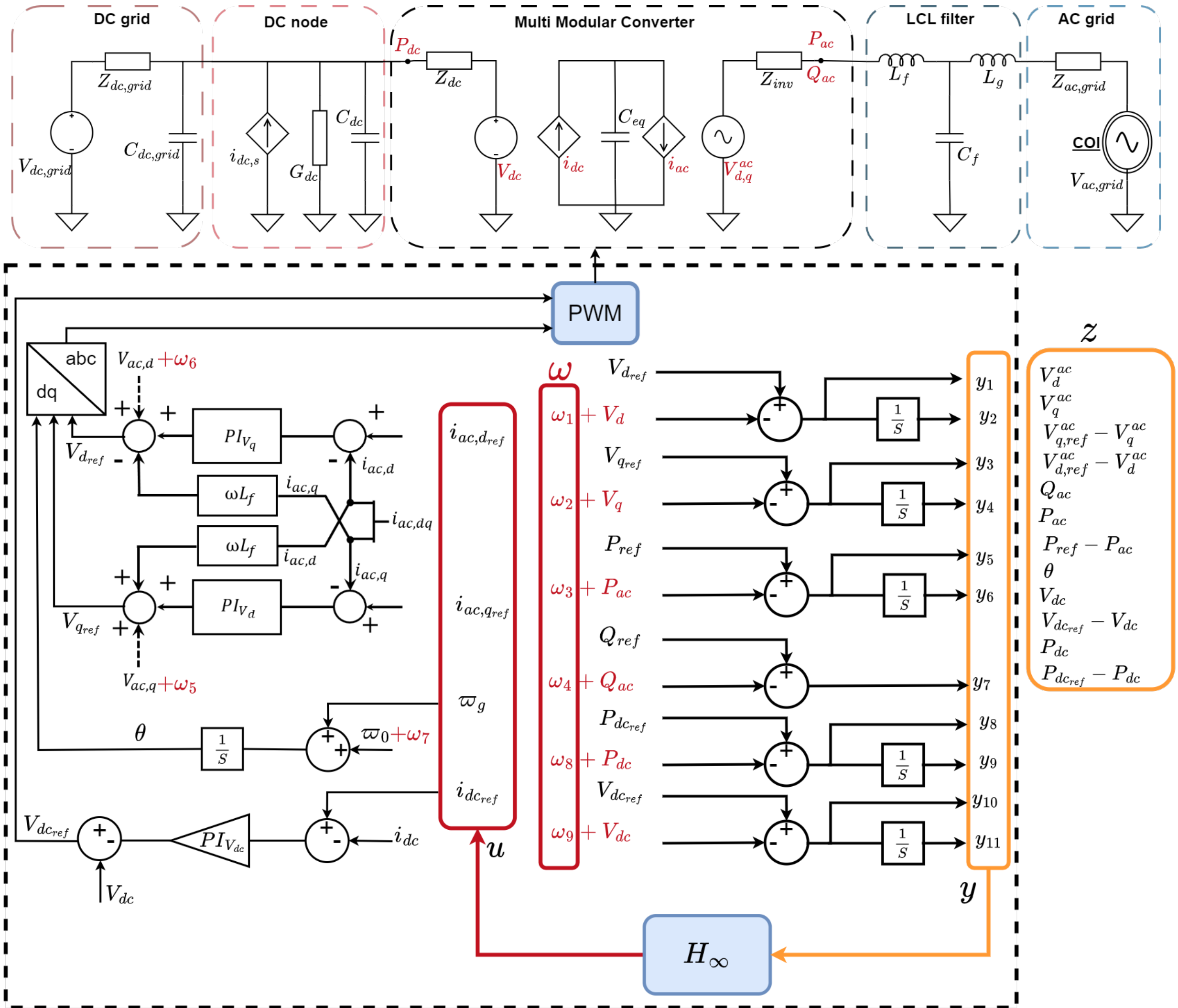

Fig. 2: Interconnection AC/DC system with a MMC in a closed loop with a H_∞ controller.

2) Grid forming Control Objectives: While there is no consensus on the definition of grid-forming, in this work we call a power converter grid-forming whenever it is able to establish and maintain the voltage and frequency of an electrical grid. In the context of AC grids, a grid-forming device is responsible for generating the necessary voltage and frequency references to establish a stable and synchronized grid operation. It actively regulates both the voltage and frequency, acting as a primary source of power in the absence of a stable grid connection or during grid disturbances. Similarly, in the case of DC grids, a grid-forming device assumes the role of establishing and controlling the voltage characteristics of the grid [10], [11]. It provides the necessary power to maintain the desired DC voltage level and ensure stable operation of the connected converters and loads. Given the aforementioned objectives, it is possible to pursue them from different perspectives and using different control structures.

To implement a double grid forming strategy, it is necessary to consider multiple signals from the AC and DC grids to evaluate the state of each grid properly. Using these signals, the converter sets voltage and angles references in order to maintain stability in the system. At the same time, in modern power systems, there are many sources of uncertainty that cannot be ignored in the controller design process. These uncertainties include variations in the power output of renewable sources and disturbances in measurements. Furthermore, the inherent coupling between apparent power, voltage and frequency leads to a Multiple Input Multiple Output (MIMO) control problem. A MIMO control approach that considers these factors makes it possible to design a more effective controller. The previously mentioned problem is well-suited for the H_∞ control framework, which guarantees adequate performance, and design flexibility regarding the objectives, and finally, guarantees stability margins [12], [13].

B. H_∞ Control Formulation and Problem

The control formulation includes a set of inputs, outputs, and performance objectives that we select depending on our control objectives, as shown later in detail in Subsection III-C.

To synthesize our controller we consider a simplified (low order and linearized) model for control design, given by:

$$\begin{bmatrix} z \\ y \end{bmatrix} = \underbrace{\begin{bmatrix} P_{11}(s) & P_{12}(s) \\ P_{21}(s) & P_{22}(s) \end{bmatrix}}_{P(s)} \begin{bmatrix} \omega \\ u \end{bmatrix} \tag{6}$$

$$u = K(s)y \tag{7}$$

where ω is the vector of inherent disturbances, u is the vector of inputs to the system, y is the vector of measured outputs of the system and z is the performance output vector. Furthermore, $P(s)$ represents the plant. H_∞ control allows us to synthesize a static controller K that achieves the desired behavior based on the objectives of the control designer. The optimization problem in H_∞ control involves minimizing the H_∞ norm of the transfer function from the disturbance inputs to the controlled outputs, subject to certain performance and stability constraints.

To compute the H_∞ norm, the transfer function matrix is first converted to a special form called the generalized plant. This involves adding weighting functions to the inputs and outputs of the transfer function to reflect the relative importance of each input and output in the system. The generalized plant is then used to form an optimization problem that seeks to find a controller that minimizes the H_∞ norm of the transfer function subject to certain constraints. From (6) and (7), we realize that the closed-loop transfer function of the system from $\omega \to z$ is

$$g(P,K) = \left[P_{11} + P_{12}K(I - P_{22}K)^{-1}P_{21}\right](j\omega) \tag{8}$$

In consequence, we are looking for a K that minimizes the weighted H_∞ norm of $g(P,K)$, such as

$$\min_{K \in H_\infty} \|Wg(P,K)\|_\infty = \min_K \max_{\omega \in \mathbb{R}} \overline{\sigma}(W(j\omega)g(P,K)) \tag{9}$$

with W being the weighting matrix. To achieve a multi-objective design, we use the approach in [12], where the matrix multiplication in (9) is replaced by an entry-wise product of matrices such as

$$\min_K \|W \circ g(P,K)\|_\infty = \min_K \max_\omega \overline{\sigma}(W(j\omega) \circ g(P,K)) \tag{10}$$

where $\circ$ is the entry-wise product. This change allows us more freedom in specifying the shaping filter of (10) and, therefore, more flexibility in the system's overall behavior.

To implement a H_∞ design, we need to define the aforementioned inputs and outputs vectors based on our control objectives as follows. Our chosen inputs to the controller are the MMC measurements in the AC and DC grid, shown in red at the MMC in Figure 2. We also consider inherent disturbances represented by the ω vector, where ω_1 to ω_4 are the disturbances for the measurements of V_d, V_q, P_{ac} and Q_{ac}. Meanwhile, ω_5 and ω_6 impact the reference calculation of V_d and V_q, ω_7 is the disturbance acting on the angle θ, and finally, ω_8 and ω_9 are the disturbances for the measurements of P_{dc}, V_{dc} respectively. To ensure proper tracking, we obtain an error signal by comparing the measurements to their references, which we integrate to calculate the steady-state error. These signals are grouped in the vector y as

$$y = \begin{bmatrix} y_1 \\ y_2 \\ y_3 \\ y_4 \\ y_5 \\ y_6 \\ y_7 \\ y_8 \\ y_9 \\ y_{10} \\ y_{11} \end{bmatrix} = \begin{bmatrix} V_{ac,d}^{ref} - V_{ac,d} + \omega_1, \\ \frac{1}{s}(V_{ac,d}^{ref} - V_{ac,d} + \omega_1) \\ V_{ac,q}^{ref} - V_{ac,q} + \omega_2, \\ \frac{1}{s}(V_{ac,q}^{ref} - V_{ac,q} + \omega_2) \\ P^{ref} - P + \omega_3, \\ \frac{1}{s}(P^{ref} - P + \omega_3), \\ Q^{ref} - Q + \omega_4, \\ V_{dc}^{ref} - V_{dc} + \omega_8, \\ \frac{1}{s}(V_{dc}^{ref} - V_{dc} + \omega_8) \\ P_{dc}^{ref} - P_{dc} + \omega_{10}, \\ \frac{1}{s}(P_{dc}^{ref} - P_{dc} + \omega_{10}) \end{bmatrix} \tag{11}$$

where $V_{ac,d}^{ref}$ and $V_{ac,q}^{ref}$ are the AC voltage reference for the direct and quadrature coordinate in the dq system respectively. Moreover, $V_{ac,d}$ and $V_{ac,q}$ are the AC voltage measurements in dq coordinates. In addition, we have P^{ref} and Q^{ref} which are the references for active and reactive AC power delivery from the converter respectively. In the same sense, we measure the active and reactive power delivered to the grid as P and Q respectively. With respect to the DC grid we have the references for voltage and power as V_{dc}^{ref} and P_{dc}^{ref} and their respective measurements as V_{dc} and P_{dc}.

One notable aspect of the approach taken is the absence of an integrator in the case of Q. The grid-forming unit is expected to control the voltage magnitude, and therefore Q is implicitly defined by the grid power flow equations. In this sense, it is important to emphasize that adding all the integrators in our control structure require that all provided setpoints for power and voltage are consistent, that is, compatible with the load flow equations for the AC and the DC grid. Such values would need to be adapted (by means of a centralized controller, for instance) should something in the grid change, e.g., changes in load or generation. Another option would rely on removing certain outputs y and their associated integrators and thereby relaxing the tracking requirements for the corresponding variables.

The controller's output is the following reference vector for AC current, frequency and DC current

$$u = [i_{ac,d_{ref}}, i_{ac,q_{ref}}, \varpi_g, i_{dc_{ref}}]^\top \tag{12}$$

which passes through a current control loop composed of several PI controllers before reaching the MMC, see Figure 2. This particular implementation allows us to tune properly how aggressively the controller behaves and also gives us extra freedom degrees to slightly correct modeling errors or disturbances not considered in the H_∞ control formulation. Furthermore, having an external control loop gives us a modularity approach that can be used for implementing new functionalities to the controller.

Finally, the performance vector z consists of carefully chosen signals from the measurements and controller inputs.

These signals enable us to assess the system's behavior when the H_∞ controller is employed. Specifically, these signals have been intentionally selected for the implementation of double grid forming controllers. They take both grid connections into account and do not make any specific assumption about stiffness of either the AC or DC grid. The selected signals encompass AC and DC voltage, power, and other relevant parameters:

$$z = [V_{ac,d}, V_{ac,q}, y_1, y_3, P, Q, \theta, y_5, V_{dc}, y_8, P_{dc}, y_{10}]^\top \quad (13)$$

This definition of z allows us to observe if the controller is effectively enforcing the value of the signals to their references. Therefore, we consider not only the measure values but also the deviation signals with respect to the references.

C. Control Objectives and Weighting Functions

In this subsection, we focus on the weighting transfer function matrix $W(s)$ that shapes the closed-loop dynamics of the system with the controller.

1) Weighting functions for H_∞control: We use weighting functions $W(s)$, also known as shaping filters, to shape the transfer function matrix of the system $P(K(s))$ considering the controller's performance. In other words, we modify the natural behavior of the system by imposing requirements through the weighting functions and, in consequence enforcing the controller objectives for the system, in our particular case, a double grid forming behavior. To choose the weighting functions, we recall the concept of sensitivities of the closed-loop system to reference signals, disturbances, and noise. We use the standard mixed sensitivity concept. Consider $S(j\omega)$ to be the output sensitivity function defined as $S(j\omega) = (I + P(j\omega)K(j\omega))^{-1}$. To ensure accurate reference tracking, we seek that $P(j\omega)K(j\omega) \gg 0$ in the low end of the frequency spectrum, given that the reference signals in power systems are much slower than the system's dynamics. Therefore, $S(j\omega)$ will be small for low frequencies and large for high frequencies. On the other end, we would like to reject inherent noise in the output measurements from the MMC. For this goal, we look at the complementary sensitivity function commonly defined as $T(j\omega) = P(j\omega)K(j\omega)(I + P(j\omega)K(j\omega))^{-1}$. In this case, we want to maintain $P(j\omega)K(j\omega)$ small at the same frequencies where the noise is concentrated, usually occurring at high frequencies. Therefore, we will minimize the noise effects on the output. Noise rejection and accurate tracking are not two conflicting objectives if the shaping filters are properly tuned; problems arise when we adjust shaping filters to have good reference tracking and noise rejection in the same frequency range, given that $S(j\omega) + T(j\omega) = I$.

2) Controller Objectives and Choice of Filters: Overall, we want to pursue the following objectives: stability and regulation in AC and DC voltage and grid synchronization. In order to achieve these objectives, we construct each map between elements of the disturbance and the performance vector z. This allows us to specify every aspect of the controller. However, the more specifications we ask for, the longer the synthesis takes, and also it is possible that there is no H_∞ controller suitable for all specifications.

The control objectives have been divided into those concerning the DC and AC grids. For each objective, we have designed a filter to help ensure optimal control performance. Specifically, we have employed a first-order filter to track references such as voltage and power.

Additionally, we have utilized a second-order filter to help mitigate the impact of disturbances on the system. This filter helps remove noise and other unwanted signals, allowing the controller to focus on the signals most relevant to achieving our control objectives. A second order filter was selected to be able to design a sharp magnitude drop around the resonance frequency of the LCL filter, therefore, the controller will reduce its impact around this frequency. Furthermore, we only use first- and second-order filters to maintain the controller's synthesis in a minimum time and make it easier to calibrate.

a) DC grid Objectives: To maintain the stability of the DC grid it is paramount to maintain the DC node voltage stable. Therefore we consider that the voltage reference should be tracked with fast dynamics, leading to the filter

$$z_{12} \to \omega_8 : \mathcal{W}_{DC,V,1} = \frac{s+5}{s + 2 \cdot 10^{-4}} \quad (14)$$

The filter above allows good tracking of the reference in low frequencies. It is aggressive given that we need to track rapidly the DC voltage references in order to maintain stability of the DC grid. Furthermore, it is also necessary to reject high-frequency disturbances from different system sources. For this end, we use the following filter to suppress high frequency disturbances on the V_{dc} reference node

$$z_{11} \to \omega_8 : \mathcal{W}_{DC,V,2} = \frac{2 \cdot 10^{-8} s^2 + 2.82 \cdot 10^{-5} s + 1}{2 \cdot 10^{-12} s^2 + 2.8 \cdot 10^{-7} s + 1}$$

Besides, we consider a filter that tracks the power needed on the DC side, in order to stabilize voltage in the DC grid:

$$z_{13} \to \omega_9 : \mathcal{W}_{DC,P} = \frac{s+20}{s + 1 \cdot 10^{-5}}.$$

In the AC grid, we have to consider several objectives which are necessary in order to have a stable AC grid. The objectives are grid synchronization, power regulation and voltage regulation, detailed below.

b) Grid Synchronization: For grid synchronization, it is paramount to be able to apply grid forming behavior on the AC side as it was imposed on the DC side. Therefore, a fast dynamic tracker filter for the reference angle θ is employed for this end:

$$z_7 \to \omega_7 : \mathcal{W}_{AC,\theta} = \frac{s+20}{s + 2 \cdot 10^{-4}} \quad (15)$$

Therefore, we accurately will track the reference θ and will impose a grid-forming algorithm.

c) Active Power Regulation: For the active power regulation, we will track accurately the active power reference,

$$z_8 \rightarrow \omega_3 : \mathcal{W}_{AC,P,1} = \frac{s+50}{s+5\cdot 10^{-4}}$$

Furthermore, in order to reject high-frequency disturbances that might occur and affect the power reference, we decide to implement the following filter

$$z_5 \rightarrow \omega_3 : \mathcal{W}_{AC,P,2} = \frac{1\cdot 10^{-6}s^2 + 1.6\cdot 10^{-3}s + 1}{2\cdot 10^{-12}s^2 + 9.9\cdot 10^{-7}s + 1}$$

As the power is affected by the grid connection, we implement the same filters to react against changes in the voltage of the AC grid in order to maintain it stable.

d) Voltage Regulation: For the voltage regulation, we would like to proceed in a similar way. But in this case, the d and q reference components should be tracked fast enough, leading us to

$$z_3 \rightarrow \omega_1 : \mathcal{W}_{AC,V_d,1} = \frac{s+20}{s+1\cdot 10^{-5}}$$

$$z_4 \rightarrow \omega_2 : \mathcal{W}_{AC,V_q,1} = \frac{s+20}{s+1\cdot 10^{-5}}$$

Furthermore, we would like to reject high-frequency disturbances, using as well a filter shape like

$$z_1 \rightarrow \omega_1 : \mathcal{W}_{AC,V_d,2} = \frac{2\cdot 10^{-8}s^2 + 2.8\cdot 10^{-5}s + 1}{2\cdot 10^{-12}s^2 + 2.8\cdot 10^{-7}s + 1}$$

$$z_2 \rightarrow \omega_2 : \mathcal{W}_{AC,V_q,2} = \frac{2\cdot 10^{-8}s^2 + 2.8\cdot 10^{-5}s + 1}{2\cdot 10^{-12}s^2 + 2.8\cdot 10^{-7}s + 1}$$

Note that $\mathcal{W}_{AC,V_d,2}$ and $\mathcal{W}_{AC,V_q,2}$ provide a magnitude drop around the resonance frequency of the LCL, which is used to reduce the control design emphasis around this frequency.

Given the previously mentioned shaping filters, and the system parameters in Table I, we use the hinfstruct routine in MATLAB to solve the H_∞ control problem in (10), and the static gain matrix K is shown in (16). As it has been previously discussed, the bandwidth of every filter have been selected depending on the objectives for each variable. We choose that $\mathcal{W}_{DC,V,1}$ in (14) have a tighter bandwidth than $\mathcal{W}_{AC,\theta}$, low enough to behave as a grid forming source. Furthermore, we use the second order filters to reject the disturbances in AC and DC, it has the magnitude drop close to 1100 Hz, which is the resonance frequency of the LCL filter.

The static matrix K in (16) reveals an important characteristic regarding the relationship between various references and measurements. Specifically, it indicates that the gain between $i_{ac,d_{ref}}$ and the variables $V_{ac,d}$, $V_{ac,q}$, and P_{ac} is close to zero. This implies that, considering the chosen weights, certain references are not significantly affected by specific measurements. In other words, we are minimizing the influence or interaction between these references and measurements in the control system.

D. Grid Forming and Grid Following Dynamics in the DC and AC grid

Qualitatively speaking, one of the fundamental characteristics of grid-forming converters is the ability to maintain a constant voltage vector despite grid events. This behavior aligns with the role of a voltage source, where the voltage magnitude and angle remain relatively constant. Consequently, when events occur in the grid, the power output of the grid-forming controller may abruptly change in response to grid conditions, in order to guarantee grid stability and synchronization with other units. It is worth noting that steady-state changes in the grid angle, caused by topological changes or load events, need to be tracked by the controller to ensure proper synchronization. On the other hand, grid-following controllers are designed to act like current sources, ensuring a consistent power output regardless of grid events. These controllers adjust their angle, often through a phase-locked loop (PLL), to maintain a constant provided current. This distinction results in a lower bandwidth for the grid-forming controller's transfer function between angle internal reference and angle disturbances caused by grid events.

In our control approach, we address the dynamics of both the AC and DC sides of the grid. On the AC side, our control strategy focuses on rejecting angle disturbances from the grid, utilizing a reduced control bandwidth compared to traditional grid following control schemes. Nonetheless, this scheme allows us to adapt our shaping filter selection to either a grid following or grid forming mode on the AC side. Conversely, on the DC side, our objective is to maintain a stable DC voltage by rejecting voltage disturbances originating from the DC grid. However, achieving this comes at the cost of modifying the current set point, and our control bandwidth is limited compared to DC grid following control schemes.

Across literature and grid requirements documents, several grid-forming controllers bandwidths are proposed by the system operators in order to integrate such inverters into the system and not jeopardize the stability or robustness of the system. The proposed tracking bandwidth for the reference angle θ is usually less than 10Hz, such as [14], whose threshold is 5Hz. With our controller, the bandwidth can be easily adjusted, making our controller flexible to meet different grid requirements.

Remark 1 (Storage Feasibility): The internal capacitance of a MMC can vary depending on the specific design and application of the converter. However, in general, the capacitance of each submodule's capacitor in an MMC can range from several hundred microfarads to several thousand microfarads. The total capacitance of the converter will depend on the number of submodules and their capacitance values, which implies that the converter can supply or absorb enough energy for several milliseconds at rated power or even more time with a lower power rate [2]. In other words, we can implement our double grid forming control strategy as long as the capacitances in the submodules are not empty.

$$K = \begin{bmatrix} 0.0042 & 3.28 & 0.07 & 1.14 & 0.0011 & 42.18 & 0.15 & -31.66 & -18.41 & 18.82 & 4.4 \\ -0.56 & -17.47 & -0.02 & -7.77 & 0.0008 & -58.3 & -0.88 & -162.28 & -10.48 & 17.48 & -0.43 \\ 17.94 & 27.04 & -47.74 & 2.03 & -12.57 & -35.43 & 0.06 & 239.54 & -3.46 & -24.02 & -29.87 \\ -70.95 & -92.53 & 12.95 & -33.98 & 252.19 & 32.4 & 2.83 & 93.07 & -0.13 & 95.64 & 23.05 \end{bmatrix} \quad (16)$$

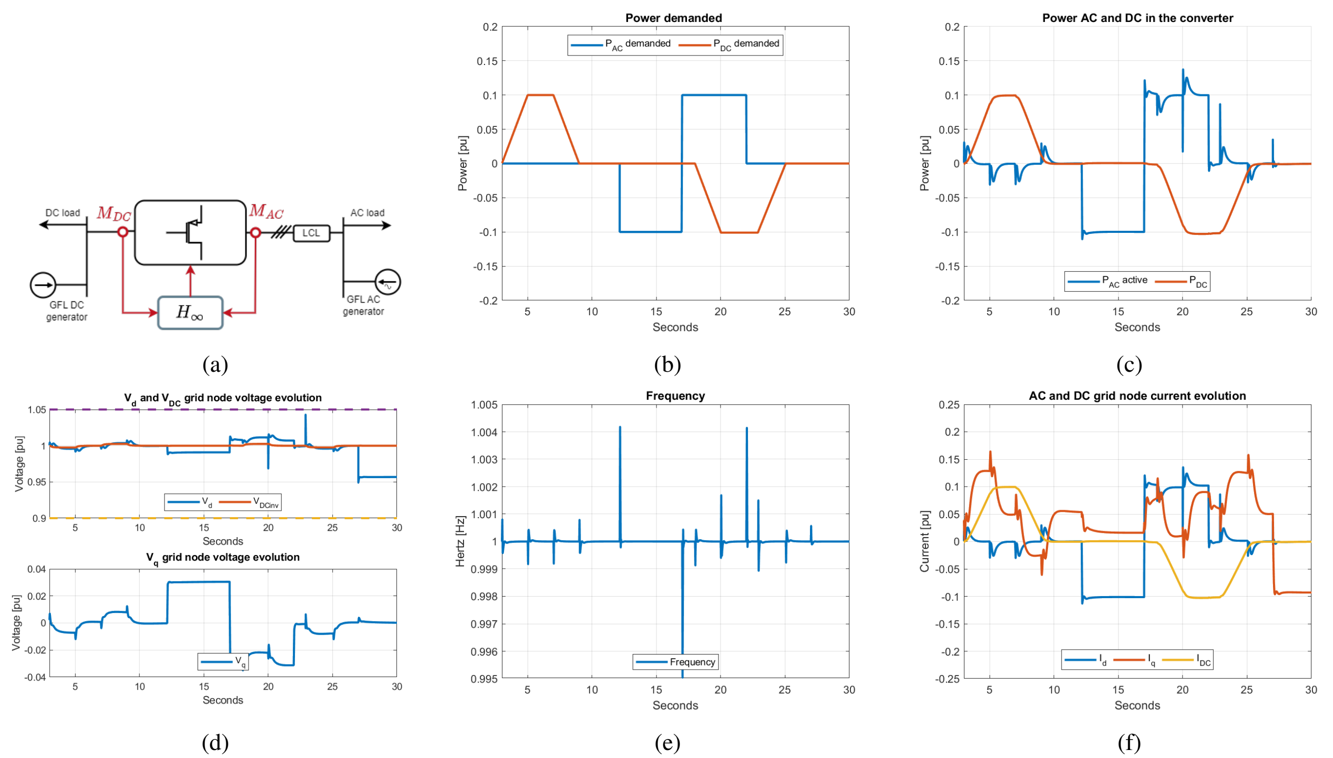

Fig. 3: (a) Model simulated (b) Power demanded (c) Power AC and DC in the converter (d)Voltage AC and DC in the inverter (e) Frequency inside the converter (f) Current AC and DC in the inverter.

TABLE I: Case Study System Parameters

Multi Modular Converter Parameters			
Parameter	**Symbol**	**Value**	**Units**
Base AC Voltage	V_{ac}	11	kV
Base DC Voltage	V_{dc}	6	kV
Power Base Value	S	100	kVA
Frequency Base Value	f	50	Hz
Converter side inductor	L_f	0.05	p.u.
LCL Capacitor	C_f	0.05	p.u.
Grid side inductor	L_g	0.05	p.u.
PI gains current control loop AC		$[1, 6]$	-
PI gains current control loop DC		$[1, 6] \cdot 10^{-3}$	-
Submodule Capacitance	$C_{dc,inv}$	0.1	p.u.

IV. Simulation Setup

We have simulated our proposed double grid forming controller using the macroscopic simulation model of a MMC with 38 sub-modules interfacing a medium voltage AC/DC grid. The test is divided into several cases and summarized into delivering or absorbing power from the AC or DC grid, considering that requests from both sides can occur simultaneously. We consider the grid in Figure 3a, where we have on the DC grid side a DC load and a DC grid following source. Moreover, we consider on the AC side an AC load and an AC grid following source after the LCL filter. Their parameters can be found in Table I.

The 30-second simulation is mainly divided into power changes and voltage reference changes. The power changes can be seen in Figure 3b, which starts with a ramp with a slope of 0.1 p.u. per second in the DC power for two seconds, reaching a maximum of 0.2 p.u., which goes down at the same rate beginning at $t = 7s$ until reaching 0 p.u. Afterward, several changes in the power demanded to occur on the AC side, which until 10 seconds was not requesting or delivering power. At 12 seconds, there is a drop of 0.1 p.u. in the power demanded by the grid, which is seconded by a step rise of 0.2 p.u. at 17 seconds. Finally, the AC power goes to 0 p.u. at 22s. Starting at 19s, we change the DC power requested to the grid in -0.1 p.u, which goes back to 0 p.u. at $t = 25s$. Meanwhile, the AC grid requested power to test the feasibility of supporting both grids simultaneously. Finally, we test how a voltage reference change might affect the system, and at $t = 27s$, we change V_{ac}^{ref} from 1 p.u.

to 0.95 p.u. It is important to highlight that in our test,the converter never enters current saturation, which will be part of future implementations.

Figure 3c shows how the proposed controller can track almost perfectly the power required for both the AC and DC grid. It is important to highlight that we are aggressively controlling the DC power, given that the dynamics of the DC grid are faster than the AC dynamics. Therefore, we see a smoother behavior on the DC power. The AC power behavior shows some peaks and irregularities on top of the power demanded by the AC grid; such irregularities are transients originating from the change of load in the DC or AC side, which affects the frequency and makes the controller react against such changes.

With respect to the voltage behavior shown in Figure 3d, we can observe that the limits established in 1.05 p.u. and 0.9 p.u. are never violated. The DC voltage regulation does not allow the DC voltage to deviate from the reference, V_{DC}^{ref} =1 p.u. more than 1% showing the strength of the proposed controller. We are designing an aggressive controller on the DC side, nonetheless a less aggressive controller may reduce the spikes in the AC sideshown in Figure 3c, specifically in P_{ac}. For the AC side, we find in the component V_d a more relaxed behavior than V_{DC}, presenting some peaks and transitory behaviors whenever there is a change in the system. Even with the step changes, the component V_d never violates the limits and deviates from the reference about 4% in the worst case. Furthermore, we observe that at $27s$, we have a voltage drop that follows the reference established in the test case.

Concerning the frequency shown in Figure 3e, we observe that changes in the system causes changes in the frequency. It is the most drastic at $17s$, which accounts for 0.2 p.u. However, the frequency is restored to reference levels in less than 0.1 seconds. Additionally, the frequency reacts to changes in the DC side, enabling the controller to modify AC set points for both the DC and AC sides simultaneously while maintaining synchronization and stability.

Finally, in Figure 3f, the current in the AC and DC grid is shown. We can highlight that the I_d component of the AC current and I_{DC} follow a similar pattern of Figure 3b and 3c as expected. However, the I_q component of the AC current has a complementary behavior, injecting reactive power to the grid in order to be able to regulate voltage in both grids and frequency. The I_q component return to steady state close to 0 p.u once the transient has died down. Furthermore, to maintain the power reference and voltage reference at $27s$, when the AC voltage reference changes, the converter draws reactive current from the grid.

Overall, the system shows promising results; power, currents, and frequency are inside the limits of the converter. An accurate and fast reaction in the AC and DC side of the system can be observed. It is noteworthy how the frequency is maintained despite all sudden changes in the converter within admissible values, which make it safe and reliable for operating in islanded hybrid AC/DC systems or in weak grids. Results show a satisfactory performance of the H_∞ controller against changes in the power requested by the MMC. It is also possible to see that the controller reacts positively against voltage drops on the AC and DC side.

V. Conclusions and Future work

This paper presents a novel control strategy for Modular Multilevel Converters (MMCs) in a double grid forming configuration. The controller regulates DC and AC voltage and frequency, offering improved performance. It relies solely on local measurements, ensuring fast and accurate tracking of references without the need for specialized tuning knowledge. Notably, the controller considers the coupling of multiple AC and DC variables to maintain safe operation within established limits. To enhance its practical applicability, future work will involve hardware-in-the-loop implementations and the integration of multimodular controllers with overcurrent protection. These advancements will provide greater flexibility in meeting diverse grid code requirements. Furthermore, the research will explore theoretical aspects, such as investigating robustness guarantees and the consideration of the energy stored in the capacitance into the controller formulation.

References

[1] A. Tayyebi, D. Grob, A. Anta, F. Kupzog, and F. Dorfler, "Frequency stability of synchronous machines and grid-forming power converters," *IEEE Journal of Emerging and Selected Topics in Power Electronics*, vol. 8, pp. 1004–1018, 6 2020.

[2] D. Groß, Sánchez-Sánchez, E. Prieto-Araujo, and O. Gomis-Bellmunt, "Dual-port grid-forming control of mmcs and its applications to grids of grids," 6 2021.

[3] F. Dörfler and D. Groß, "Control of low-inertia power systems," *Annual Reviews in Control*, 2022.

[4] S. D. Tavakoli, S. Fekriasl, E. Prieto-Araujo, J. Beerten, and O. Gomis-Bellmunt, "Optimal $\mathcal{H}_\infty$ control design for mmc-based hvdc links," *IEEE Transactions on Power Delivery*, vol. 37, no. 2, pp. 786–797, 2022.

[5] F. Paganini and E. Mallada, "Global analysis of synchronization performance for power systems: Bridging the theory-practice gap," *IEEE Transactions on Automatic Control*, vol. 65, pp. 3007–3022, 7 2020.

[6] P. Kundur, *Power System Stability and Control*, ser. EPRI power system engineering series. McGraw-Hill Education, 1994.

[7] N. H. van der Blij, L. M. Ramirez-Elizondo, M. T. Spaan, and P. Bauer, "A state-space approach to modelling dc distribution systems," *IEEE Transactions on Power Systems*, vol. 33, pp. 949–950, 2018.

[8] E. Prieto-Araujo, A. Junyent-Ferré, C. Collados-Rodríguez, G. Clariana-Colet, and O. Gomis-Bellmunt, "Control design of modular multilevel converters in normal and ac fault conditions for hvdc grids," *Electric Power Systems Research*, vol. 152, pp. 424–437, 11 2017.

[9] H. Saad, S. Dennetière, and J. Mahseredjian, "On modelling of mmc in emt-type program." Institute of Electrical and Electronics Engineers Inc., 8 2016.

[10] M. Chen, D. Zhou, A. Tayyebi, E. Prieto-Araujo, F. Dörfler, and F. Blaabjerg, "Generalized multivariable grid-forming control design for power converters," *IEEE Transactions on Smart Grid*, 9 2021.

[11] M.-S. Debry, G. Denis, and T. Prevost, "Characterization of the grid-forming function of a power source based on its external frequency smoothing capability," in *2019 IEEE Milan PowerTech*, 2019, pp. 1–6.

[12] L. Huang, H. Xin, and F. Dörfler, "H-infinity-control of grid-connected converters: Design, objectives and decentralized stability certificates," *IEEE Transactions on Smart Grid*, vol. 11, pp. 3805–3816, 9 2020.

[13] S. Yang, Q. Lei, F. Z. Peng, and Z. Qian, "A robust control scheme for grid-connected voltage-source inverters," *IEEE Transactions on Industrial Electronics*, vol. 58, pp. 202–212, 1 2011.

[14] National Grid UK, "Great britain grid forming best practice guide," April 2023. [Online]. Available: https://www.nationalgrideso.com/document/278491/download